Neural Field Model for Measuring and Reproducing Time Intervals

Weronika Wojtak[1,2(✉)], Flora Ferreira[1], Estela Bicho[1], and Wolfram Erlhagen[2]

[1] Research Centre Algoritmi, University of Minho, Guimarães, Portugal
{w.wojtak,fjferreira,estela.bicho}@dei.uminho.pt
[2] Research Centre of Mathematics, University of Minho, Guimarães, Portugal
wolfram.erlhagen@math.uminho.pt

Abstract. The continuous real-time motor interaction with our environment requires the capacity to measure and produce time intervals in a highly flexible manner. Recent neurophysiological evidence suggests that the neural computational principles supporting this capacity may be understood from a dynamical systems perspective: Inputs and initial conditions determine how a recurrent neural network evolves from a "resting state" to a state triggering the action. Here we test this hypothesis in a time measurement and time reproduction experiment using a model of a robust neural integrator based on the theoretical framework of dynamic neural fields. During measurement, the temporal accumulation of input leads to the evolution of a self-stabilized bump whose amplitude reflects elapsed time. During production, the stored information is used to reproduce on a trial-by-trial basis the time interval either by adjusting input strength or initial condition of the integrator. We discuss the impact of the results on our goal to endow autonomous robots with a human-like temporal cognition capacity for natural human-robot interactions.

Keywords: Neural field model · Interval timing · Neural integrator

1 Introduction

Our successful interaction with an inherently dynamic environment requires the capacity to perceive elapsed time and to produce highly timed motor responses. Humans and other animals are able to generate time intervals in the range of tens of milliseconds to several seconds in anticipation of sensory events (e.g., a color change of a traffic light) without a clock or any external device [6,11]. Moreover, the temporal control of behavior often shows a striking flexibility [15], allowing the adjustment of movement initiation time based on a single or very few observations of environmental changes (e.g. a prolonged amber phase). How the nervous system manages to flexibly process temporal information in the service of behavioral goals is currently an active research field (for a recent review see [14]). A recent experiment in which monkeys were trained to measure

I. V. Tetko et al. (Eds.): ICANN 2019, LNCS 11727, pp. 327–338, 2019.
https://doi.org/10.1007/978-3-030-30487-4_26

different sample intervals (demarcated by two time markers) and immediately afterward reproduce it by a proactive saccade to a predefined target, reveals new insights into the neural processing mechanisms [8]. The main finding during the production epoch is a monotonic increase of neural population activity to a fixed threshold value associated with saccade onset. Such a ramp-to-threshold dynamics has been described previously in a wide range of brain areas during timing tasks [14]. The interesting novelty of this study is the observation that the population activity at the end of the measuring epoch (ME) predicts on a trial-by-trial basis the buildup rate during the production epoch (PE) and consequently anticipates the time of the upcoming motor response. Longer sample intervals are associated with higher firing rates at the end of ME and shallower buildup rates during PE.

Most computational models of ramping activity explain the accumulation of temporal evidence as a result of a network mechanism in which positive and negative feedback is mediated by recurrent connections between neurons [16,18]. However, well known problems with these integrator models are the requirement to fine tune network connections and the lack of robustness to perturbations [10]. Moreover, changes in the network structure (e.g., through Hebbian synaptic modification) are assumed to tune the slope of ramping activity to a new sample interval [16]. Here we use a novel model of a robust neural integrator [22] based on the theoretical framework of dynamic neural fields [17] to test a dynamical systems view on flexible measurement and reproduction of time intervals [15]. The basic assumption is that temporal flexibility can be readily understood in terms of inputs and initial conditions that control the speed with which the neural population activity in the recurrent network evolves. Our primary goal is not to explain in detail the experimental data in [8], but to investigate in numerical model simulations neuro-inspired processing mechanism that may be used in the future to endow autonomous robots with a sophisticated action timing capacity for more natural human-robot interactions [3,5].

2 Dynamic Neural Field (DNF) Model

DNF models explain the existence of self-sustained neural population activity which is commonly believed to represent a neural substrate for higher cognitive functions necessary to fill the gap between sensation and action. They have been used to model aspects of working memory, decision making, planning or learning [17] and to synthesize these cognitive skills in autonomous robots [4]. In the applications, neural fields are typically spanned over continuous dimensions such as direction, position or color. Following the experimental setup in [8], we assume for the present study that the neurons in the field represent the target of the saccadic eye movement triggered at the end of PE which is identified by movement direction. The presentation of the target input triggers the evolution of a localized activation pattern or bump encoding the specific parameter value. To represent not only the nature of the input but also the accumulation of temporal evidence we have to assume that the recurrent interactions between

the neurons in the field are able to stabilize a bump solution with a continuum of amplitudes. To ensure this we employ a novel field model [22] consisting of two coupled field equations of classical Amari type [1]. It governs the temporal evolution of two populations, $u(x,t)$ and $v(x,t)$, where x indicates the field position and t represents time:

$$\frac{\partial u(x,t)}{\partial t} = -u(x,t) + v(x,t) + \int_\Omega w(|x-y|) f(u(y,t)-h)\mathrm{d}y + S(x,t) + \epsilon^{1/2}\mathrm{d}W(x,t), \quad (1a)$$

$$\frac{\partial v(x,t)}{\partial t} = -v(x,t) + u(x,t) - \int_\Omega w(|x-y|) f(u(y,t)-h)\mathrm{d}y, \quad (1b)$$

where $w(|x-y|)$ denotes the distant-dependent connectivity kernel and $f(u)$ is the firing rate function taken here as a Heaviside step function with threshold h. This ensures that only neurons with suprathreshold activity, $f(x) = 1$ for $x \geq h$, contribute to the recurrent excitatory and inhibitory interactions. The function $S(x,t)$ represents the time varying external input to population u. The additive noise term $\mathrm{d}W(x,t)$ describes the increment of a spatially dependent Wiener process with noise amplitude $\epsilon \ll 1$. It allows us, in principle, to test predictions about the variability of time measurements, an interesting issue that goes beyond the scope of this paper.

The lateral inhibition type connectivity kernel has a "Mexican-hat" shape given by the difference of two Gaussians

$$w(x) = A_{ex} e^{\left(-x^2/2\sigma_{ex}^2\right)} - A_{in} e^{\left(-x^2/2\sigma_{in}^2\right)} - g_{in}, \quad (2)$$

with $A_{ex} > A_{in} > 0$, $\sigma_{in} > \sigma_{ex} > 0$, and a constant inhibition $g_{in} > 0$. The parameter values used throughout this study are $A_{ex} = 3$, $A_{in} = 1.5$, $\sigma_{ex} = 1$, $\sigma_{in} = 3$, $g_{in} = 0.5$.

We apply the same coupling function to the v-field with a negative sign. The shape of the distance-dependent synaptic strengths thus represents an inverted Mexican-hat with inhibition dominating at shorter and excitation at longer distances.

Numerical simulations of the model were done in Julia [2] using a forward Euler method with time step $\Delta_t = 0.001$ and spatial step $\Delta_x = 0.005$, on a finite domain Ω with length $L = 60$. To compute the spatial convolution of w and f we employ a fast Fourier transform (FFT), using Julia's package `FFTW` with functions `fft` and `ifft` to perform the Fourier transform and the inverse Fourier transform, respectively.

3 Simulation Results

In the following numerical examples, we consider a target input given by the Gaussian function

$$S(x) = A_S e^{\left(-(x-x_c)^2/2\sigma_S^2\right)}, \quad (3)$$

centered at position $x_c = 0$, with standard deviation $\sigma_S = 2$. The input strength, A_S, differs for the time interval measurement and the time interval reproduction

epochs of the experiment (see below). For simplicity, we assume that the interval to measure is defined by the duration of the external input and not by two additional time markers like in the experiments. We leave the interesting issue of potential differences in subjective time measurements with "filled" intervals as opposed to "unfilled" intervals demarcated by time markers for future studies [21]. The temporal integration process thus starts from a homogeneous activity baseline when at time $t = 0$ the suprathreshold target input is presented. Following [8], we use for the numerical tests time intervals in the range of 500 to 1000 ms.

For the reproduction epoch we distinguish two situations. (1) Like for the measurement epoch, the temporal accumulation process starts from a homogeneous initial condition with the presentation of the target input. The input strength is inversely proportional to the bump amplitude reached during ME. (2) The evolution of the population activity starts without external input from a non-homogeneous initial condition. The pre-activation of neurons representing the target direction is inversely proportional to the bump amplitude reached during ME.

3.1 Measuring Time Intervals

The following simulations illustrate how the neural trajectory in the u-field evolves in response to the localized external input specifying the target direction. Figure 1 depicts three examples of steady state solutions that are the result of the temporal input integration over different time intervals. The shape of the self-stabilized bumps reflects the fact that a longer accumulation time results in a higher bump amplitude. A closer inspection of the duration-height dependency using more time intervals reveals that the relationship is approximately linear (Fig. 2).

3.2 Reproducing Time Intervals - Varying Inputs

For the reproduction epoch we apply the same external input, $S(x, t)$, like for the time interval measurement but chose in accordance with the qualitative experimental findings in [8] the input strength in dependence of the bump amplitude reached in ME. The following relation is used for the model simulations:

$$A_S = \frac{1}{\ln(u_{max})}, \tag{4}$$

where u_{max} is maximum of the steady state solution in the u-field in the preceding measurement epoch. Figure 3 shows the input amplitudes, A_S, for the range of measured intervals. The application of the suprathreshold input triggers in all cases the evolution of a bump solution. Figure 4 compares the evolution of population activity for all tested intervals. As can be clearly seen when comparing the slopes of the curves, input strength controls the time course of the neural trajectories. Since the strength of the input is inversely proportional (on a

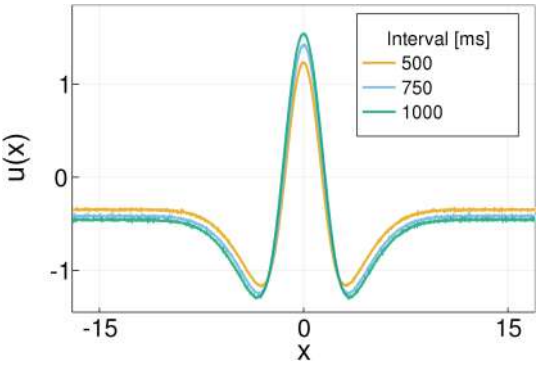

Fig. 1. Example of three steady state solutions of the u-field of (1) resulting from applying three sample intervals of durations $d_{s_j} \in \{500, 750, 1000\}$, respectively. The amplitude of the external input given by (3) is $A_S = 1.75$, the threshold for the Heaviside function $f(u)$ is $h = 0.25$.

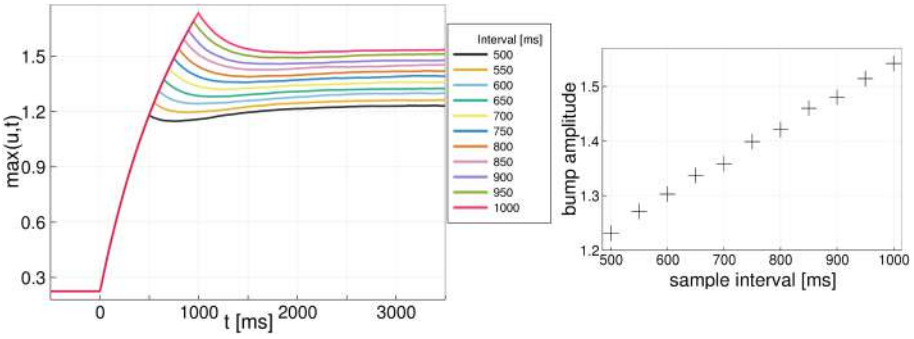

Fig. 2. Left: Time courses of activity in the u-field during the interval measuring epoch. Right: Bump amplitude at the end of the measuring epoch as a function of sample interval length.

logarithmic scale) to interval length, population activity resulting from stronger inputs will reach the fixed read-out threshold, $h_R = 2$, earlier, producing shorter time intervals for movement initiation. Conversely, localized activity integrating weaker inputs reach this threshold later in time, resulting in longer production intervals. After reaching the threshold, h_R, the activity in both fields is reset to the initial resting state. The production interval is measured as the interval between the onset of the input $S(x, t)$ at $t = 0$ and the time when the u-activity reaches the threshold.

Figure 5 compares directly the values of measured and produced intervals. For the tested range, the results reveal a very good match with a slight overestimation of the shortest intervals and a slight underestimation of the longest intervals (see also Table 1).

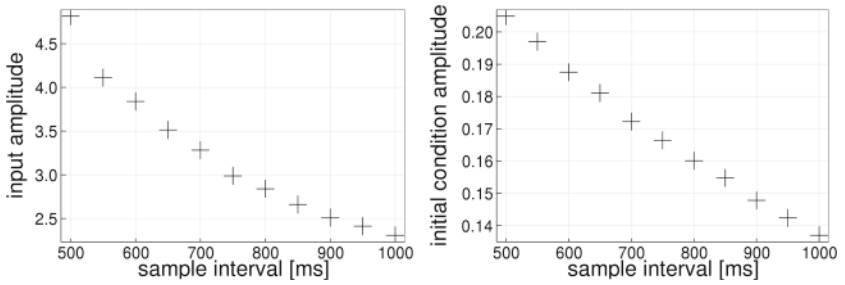

Fig. 3. Left: Strength of the input during the interval production epoch as a function of sample interval length. Right: Strength of the initial condition during the interval production epoch as a function of sample interval length.

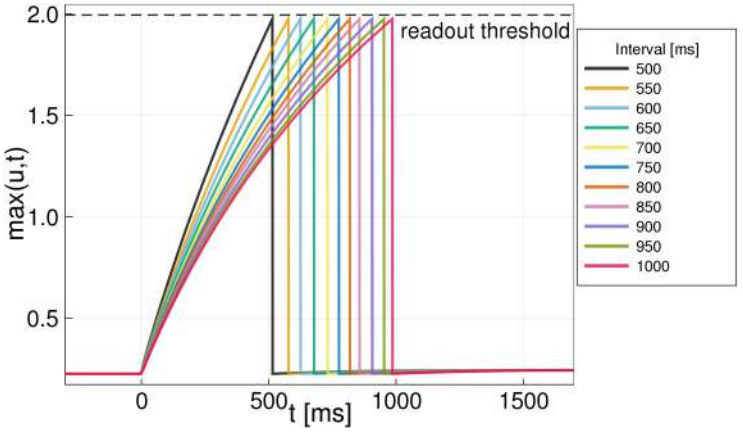

Fig. 4. Time courses of activity in the u-field during the interval production epoch. Threshold reaching time is determined by the input strength.

3.3 Reproducing Time Intervals - Varying Initial Conditions

To test the hypothesis that an adequate choice of initial condition for the population dynamics of the reproduction epoch may be sufficient to account for a flexible reproduction of measured time intervals, we proceed as follows. The numerical simulations do not start from a homogeneous resting state. Instead, the population centered at position x_c representing the planned movement direction appears to be pre-activated at time $t = 0$. The amplitude of the preshape depends on the outcome of the preceding measuring epoch in the following manner:

$$u(x,0) = \frac{1}{\alpha e^{(u_{max})}} e^{\left(-(x-x_c)^2/8\right)}, \qquad v(x,0) = K - u(x,0), \tag{5}$$

where u_{max} is maximum activity of the steady state solution in the u-layer reached during ME, and α is a constant scaling factor for the preshape ampli-

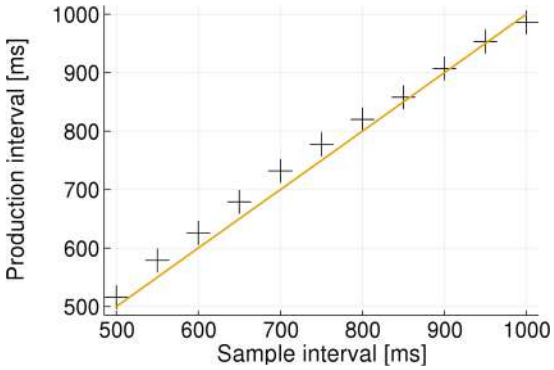

Fig. 5. Production intervals as a function of sample intervals. Goodness of fit $R^2 = 0.99$.

tude which decreases with increasing u_{max}. The role of the constant K can be understood by noting that the subthreshold population dynamics ($f(u) = 0$) has the equilibrium solution $u(x) = v(x)$. By choosing $K > 2h$ one can ensure that the dynamics of the coupled populations will reach the threshold h necessary to drive the evolution of a bump. For the numerical tests we use $K = 0.5$, $h = 0.22$ and $\alpha = 1.25$. The initial condition may be set for instance by a transient input controlling the bell-shaped pre-activation and by a transient "go" signal (e.g., the second flash in the monkey experiment) controlling K and consequently the onset of the temporal evolution at $t = 0$. Figure 6 shows the time course of activity of the u-population for all measured intervals. The initial preshape amplitude predicts motor timing. Stronger preshapes are associated with shorter production intervals. Since no external input is applied, the neural trajectory is identical for all intervals once the threshold for the bump formation is reached. The difference in timing is thus completely explained by the speed with which the subthreshold trajectory reaches threshold, which in turn is determined by the activation gap between $u(x, 0)$ and h. Figure 7 directly compares the measured and produced intervals. The coefficient of determination, $R^2 = 0.95$, indicates that the numerical results fit still quite well the model of a perfect measuring/production match, albeit with larger errors compared to the model with external input (see also Table 1).

Table 1. Values (in milliseconds) of sample and produced intervals.

Sample interval	500	550	600	650	700	750	800	850	900	950	1000
Produced interval (external inputs)	516	579	626	679	732	777	820	858	907	953	986
Produced interval (initial conditions)	518	604	676	741	793	820	862	893	923	950	972

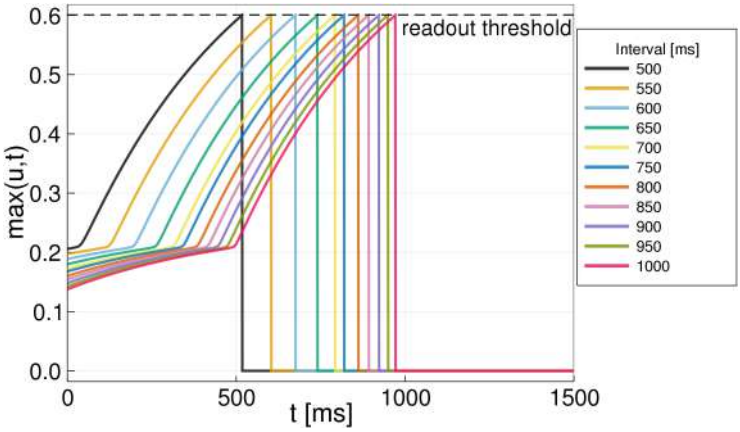

Fig. 6. Time courses of activity in the u-field during the interval production epoch. The instants of reaching the read-out threshold, $h_R = 0.6$, vary systematically in dependence of the initial condition of the field dynamics.

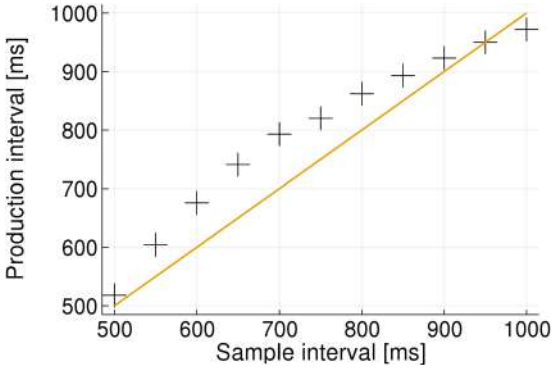

Fig. 7. Production intervals as a function of sample intervals. Goodness of fit $R^2 = 0.95$.

4 Discussion

The results of our simulation study support the notion that neural computational principles of flexible timing may be captured by a dynamical systems perspective. Closely balanced excitation and inhibition in a spatially structured neural network explain the temporal integration and maintenance of external inputs. The information about elapsed time stored in the bump amplitude can be used on a trial-by-trial basis to reproduce the time interval either by adjusting input strength or initial condition of the neural integrator. This affects the speed or the onset of the neural trajectory towards the bump attractor, respectively. The field model shares with other recurrent network models the assumption that the

neural mechanisms for timing are closely integrated with the processing of other stimulus attributes like for instance movement direction [12,14].

There are several open issues with the current model implementation. First of all, since the input is continuously integrated, not only its duration but also its strength will influence the bump amplitude and consequently the interval measurement. The "strength normalization" issue can be solved by not integrating the input directly but instead a bump from a connected neural field which is triggered and deleted by transient signals (e.g., input onset and offset). In classical neural field models, the shape of such a memory bump is exclusively determined by the recurrent interactions within the network [1,4]. Moreover, recurrent interactions are known to increase the signal-to-noise ratio, making the integration process more robust compared to the direct integration of a potentially weak and noisy input. Interestingly, the usage of a memory bump in the integration process might also explain the finding that "filled" intervals are typically judged as lasting longer than "unfilled" intervals of the same duration [21]. Since a stationary bump solution of the field equation with a lasting external input has a slightly larger amplitude compared to a bump triggered by a brief, transient input, the temporal integration in the "filled" condition predicts a larger bump amplitude in the measurement field compared to the "unfilled" condition.

A second issue concerns the scaling of intervals to values outside the measured range by instruction or symbolic cues [20]. The effective bump height during reproduction should reflect this additional information. We have recently proposed and tested a simple and effective adaptation rule for the bump height based on the comparison between the produced time course of population activity and the neural trajectory of a reference or synchronization signal indicating the expected timing [23].

Our ultimate application goal for the model is to advance towards a human-like temporal cognition capacity for autonomous robots [13]. We are planning to test the model as part of an existing dynamic field control architecture for natural human-robot cooperation [5]. The continuous real-time synchronization of decision and actions with a human partner requires flexible perception and production of time intervals, fully integrated in other cognitive processes without reference to external computer clocks. A concrete example of human-robot collaboration is an assembly paradigm in which a robot assistant hands over a series of objects to the human worker. Findings in recent experiments directly comparing human-human and human-robot handovers stress the importance of temporal aspects of the robot's actions [7,9]. Being able to adapt to the user by minimizing the human's waiting time is considered crucial for user acceptance and satisfaction. Figure 8 presents a sketch of a possible model implementation in the context of a cooperative object transfer task. The robot has first to measure the duration of individual assembly steps. This could be achieved for instance in a learning by demonstration paradigm in which the robot watches a human teacher executing the assembly work (assuming that all objects are within reach, [19]). Time measurement starts when the robot observes the teacher reaching for a specific object and stops when he/she reaches for the next one. The input to the

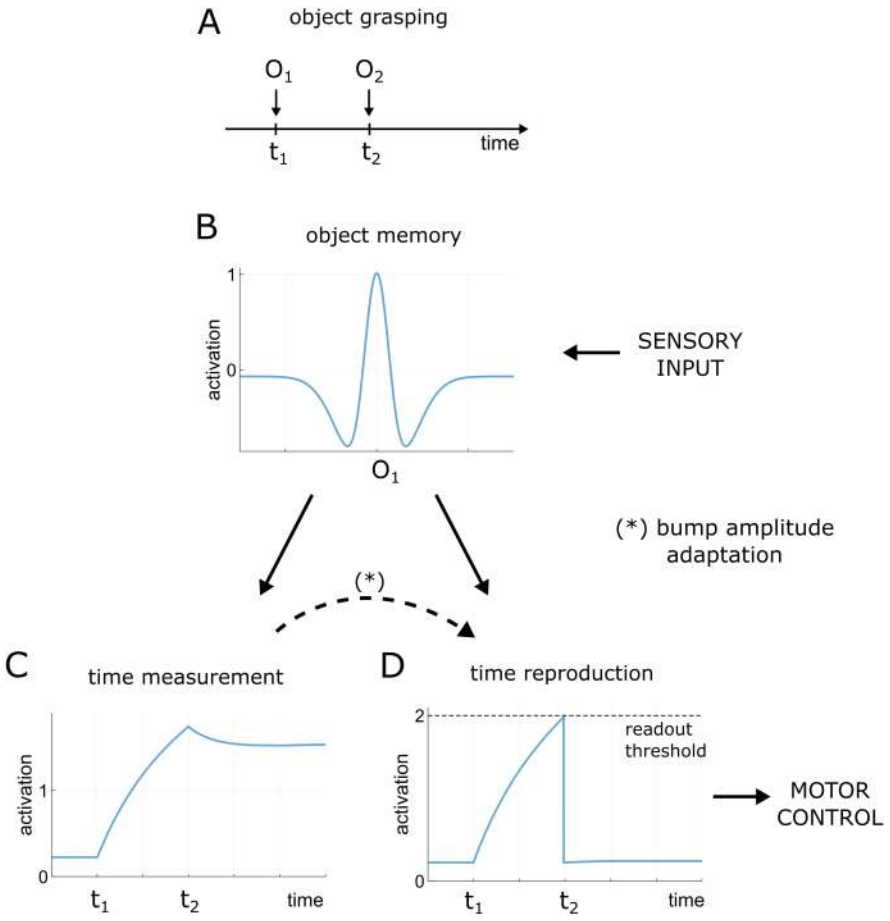

Fig. 8. Object handover task. (A) The robot has to measure the time interval, $[t_1, t_2]$, between two consecutive graspings of object O_1 and object O_2. (B) Visual input from the camera system, characterizing the first object (e.g., object color), drives the evolution of a bump in an object memory field. (C) Time course of the temporal integration of the object memory in the measurement field during the interval $[t_1, t_2]$. (D) The measured duration is recalled in the reproduction field by integrating the memory bump with an amplitude defined by the measurement bump in (C). Reaching the readout threshold is associated with the initiation of the object transfer to the exchange position.

measurement field is thus a self-stabilized bump in a memory field representing the object currently manipulated. During joint task execution, the robot uses the temporal information stored in the bump amplitude to prepare the complementary action of holding out the next object for the user. The temporal integration of the object memory bump with an amplitude given by Eq. 4 causes ramping activity in the time reproduction field. Reaching the pre-defined activation

threshold at the end of the interval to be estimated is associated with the initiation of the object transport to the exchange position. Due to motor delays, the object exchange may still not be in perfect synchrony. A perceived temporal mismatch between the expected and the realized event timing (e.g., user picking object from robot hand) can be used to adapt in a single trial the initial resting state in the reproduction field in order to compensate systematic motor delays [23]. We are currently studying how the choice of the time scale of the robust neural integrator ($\tau = 1$ in the present study) affects precision timing for time intervals that are relevant for human-robot interactions.

Acknowledgments. The work received financial support from FCT through the PhD fellowship PD/BD/128183/2016, the project "Neurofield" (POCI-01-0145-FEDER-031393) and the research centre CMAT within the project UID/MAT/00013/2013.

References

1. Amari, S.: Dynamics of pattern formation in lateral-inhibition type neural fields. Biol. Cybern. **27**(2), 77–87 (1977). https://doi.org/10.1007/BF00337259
2. Bezanson, J., Edelman, A., Karpinski, S., Shah, V.B.: Julia: a fresh approach to numerical computing. SIAM Rev. **59**(1), 65–98 (2017). https://doi.org/10.1137/141000671
3. Bicho, E., Louro, L., Erlhagen, W.: Integrating verbal and nonverbal communication in a dynamic neural field architecture for human-robot interaction. Front. Neurorobotics **4**, 5 (2010). https://doi.org/10.3389/fnbot.2010.00005
4. Erlhagen, W., Bicho, E.: The dynamic neural field approach to cognitive robotics. J. Neural Eng. **3**, 36–54 (2006). https://doi.org/10.1088/1741-2560/3/3/R02
5. Erlhagen, W., Bicho, E.: A dynamic neural field approach to natural and efficient human-robot collaboration. In: Coombes, S., beim Graben, P., Potthast, R., Wright, J. (eds.) Neural Fields, pp. 341–365. Springer, Heidelberg (2014). https://doi.org/10.1007/978-3-642-54593-1_13
6. Gallistel, C.R., Gibbon, J.: Time, rate, and conditioning. Psychol. Rev. **107**(2), 289–344 (2000). https://doi.org/10.1037//0033-295X.107.2.289
7. Glasauer, S., Huber, M., Basili, P., Knoll, A., Brandt, T.: Interacting in time and space: investigating human-human and human-robot joint action. In: RO-MAN, 2010 IEEE, pp. 252–257. IEEE (2010). https://doi.org/10.1109/ROMAN.2010.5598638
8. Jazayeri, M., Shadlen, M.N.: A neural mechanism for sensing and reproducing a time interval. Curr. Biol. **25**(20), 2599–2609 (2015). https://doi.org/10.1016/j.cub.2015.08.038
9. Koene, A., et al.: Relative importance of spatial and temporal precision for user satisfaction in human-robot object handover interactions. In: Proceedings of the New Frontiers in Human-Robot Interaction, vol. 14 (2014)
10. Lim, S., Goldman, M.S.: Balanced cortical microcircuitry for maintaining information in working memory. Nat. Neurosci. **16**(9), 1306 (2013). https://doi.org/10.1038/nn.3492
11. Machado, A., Malheiro, M.T., Erlhagen, W.: Learning to time: a perspective. J. Exp. Anal. Behav. **92**(3), 423–458 (2009). https://doi.org/10.1901/jeab.2009.92-423

12. Machens, C.K., Romo, R., Brody, C.D.: Functional, but not anatomical, separation of "what" and "when" in prefrontal cortex. J. Neurosci. **30**(1), 350–360 (2010). https://doi.org/10.1523/JNEUROSCI.3276-09.2010
13. Maniadakis, M., Trahanias, P.: Temporal cognition: a key ingredient of intelligent systems. Front. Neurorobotics **5**, 2 (2011). https://doi.org/10.3389/fnbot.2011.00002
14. Paton, J.J., Buonomano, D.V.: The neural basis of timing: distributed mechanisms for diverse functions. Neuron **98**(4), 687–705 (2018). https://doi.org/10.1016/j.neuron.2018.03.045
15. Remington, E.D., Egger, S.W., Narain, D., Wang, J., Jazayeri, M.: A dynamical systems perspective on flexible motor timing. Trends Cogn. Sci. **22**(10), 938–952 (2018). https://doi.org/10.1016/j.tics.2018.07.010
16. Reutimann, J., Yakovlev, V., Fusi, S., Senn, W.: Climbing neuronal activity as an event-based cortical representation of time. J. Neurosci. **24**(13), 3295–3303 (2004). https://doi.org/10.1523/JNEUROSCI.4098-03.2004
17. Schöner, G., Spencer, J.: Dynamic Thinking: A Primer on Dynamic Field Theory. Oxford University Press, Oxford (2016). https://doi.org/10.1093/acprof:oso/9780199300563.001.0001
18. Simen, P., Balci, F., deSouza, L., Cohen, J.D., Holmes, P.: A model of interval timing by neural integration. J. Neurosci. **31**(25), 9238–9253 (2011). https://doi.org/10.1523/JNEUROSCI.3121-10.2011
19. Sousa, E., Erlhagen, W., Ferreira, F., Bicho, E.: Off-line simulation inspires insight: a neurodynamics approach to efficient robot task learning. Neural Netw. **72**, 123–139 (2015). https://doi.org/10.1016/j.neunet.2015.09.002
20. Wang, J., Narain, D., Hosseini, E.A., Jazayeri, M.: Flexible timing by temporal scaling of cortical responses. Nat. Neurosci. **21**(1), 102 (2018). https://doi.org/10.1038/s41593-017-0028-6
21. Wearden, J.H., Norton, R., Martin, S., Montford-Bebb, O.: Internal clock processes and the filled-duration illusion. J. Exp. Psychol. Hum. Percept. Perform. **33**(3), 716 (2007). https://doi.org/10.1037/0096-1523.33.3.716
22. Wojtak, W., Coombes, S., Bicho, E., Erlhagen, W.: Combining spatial and parametric working memory in a dynamic neural field model. In: Villa, A.E.P., Masulli, P., Pons Rivero, A.J. (eds.) ICANN 2016. LNCS, vol. 9886, pp. 411–418. Springer, Cham (2016). https://doi.org/10.1007/978-3-319-44778-0_48
23. Wojtak, W., Ferreira, F., Erlhagen, W., Bicho, E.: Learning joint representations for order and timing of perceptual-motor sequences: a dynamic neural field approach. In: 2015 International Joint Conference on Neural Networks (IJCNN), pp. 3082–3088. IEEE (2015). https://doi.org/10.1109/IJCNN.2015.7280717